Neuroblastoma tumorigenesis is regulated through the Nm23-H1/ h-Prune C-terminal interaction

Marianeve Carotenuto[1,2], Emilia Pedone[3#], Donatella Diana[3#], Pasqualino De Antonellis[1,2#] Sašo Džeroski[7], Natascia Marino[1,14], Luigi Navas[5], Valeria Di Dato[1,2], Maria Nunzia Scoppettuolo[1,2], Flora Cimmino[1,2], Stefania Correale[3], Luciano Pirone[13], Simona Maria Monti[3], Elisabeth Bruder[6], Bernard Ženko[7], Ivica Slavkov[7], Fabio Pastorino[8], Mirco Ponzoni[8], Johannes H. Schulte[9], Alexander Schramm[9], Angelika Eggert[9], Frank Westermann[10], Gianluigi Arrigoni[11], Benedetta Accordi[12], Giuseppe Basso[12], Michele Saviano[13], Roberto Fattorusso[3-4], Massimo Zollo[1,2,] *.

[#] These authors contributed equally to the work

First author: Marianeve Carotenuto

1 Centro di Ingegneria Genetica e Biotecnologie Avanzate (CEINGE), Naples, Italy
2 Dipartimento di Biochimica e Biotecnologie Mediche, Universita` 'Federico II' di Napoli, Italy
3 Istituto di Biostrutture e Bioimmagini, CNR, Napoli, Italy
4 Dipartimento di Scienze Ambientali, Seconda Universita` di Napoli, Caserta, Italy
5 Sezione di Clinica Chirurgica, Dipartimento di Scienze Cliniche Veterinarie, Università Federico II' di Napoli, Naples, Italy
6 Department of Pathology, University of Basel, Basel, Switzerland.
7 Department of Knowledge Technologies, Jožef Stefan Institute, Jamova cesta 39, 1000 Ljubljana, Slovenia
8 Istituto Giannina Gaslini, Ospedale Pediatrico, 16148 Genoa, Italy
9 Department of Paediatric Oncology and Haematology, University Children's Hospital Essen, 45122 Essen, Germany
10 Department of Tumour Genetics, German Cancer Research Centre, Heidelberg, Germany
11 Department of Pathology, Ospedale San Raffaele, Milan, Italy
12 Haemato-Oncology Laboratory, Department of Paediatrics, University of Padova, Padua, Italy
13 Istituto di Cristallografia CNR, Bari, Italia
14 Women's Cancers Section, Laboratory of Molecular Pharmacology, National Cancer Institute, Bethesda, USA

*** Corresponding Author: Massimo Zollo**
Dipartimento di Biochimica e Biotecnologie Mediche
University 'Federico II' of Naples
Via Pansini 5, 80131 Naples, Italy
Centro di Ingegneria Genetica e Biotecnologie Avanzate (CEINGE), Via Gaetano Salvatore 486, 80145 Naples, Italy
Phone +390813737875
Fax: +390813737711
e-mail: massimo.zollo@unina.it

Supplementary Information

C-terminal region of h-Prune enhances cell motility (Supplementary Fig. 1a-e)

We determined the effects of dipyridamole and we found that it did not affect cell motility of two NBL cell lines (SH-SY5Y and SK-N-BE cells) (data not shown). This thus supported our hypothesis that only the formation of the protein complex between Nm23-H1 and h-Prune can promote the observed increased cellular motility. Then, we independently assayed the N-terminal and C-terminal regions of h-Prune using specific constructs transfected into HEK293 and SH-SY5Y cells (for description of constructs, see Kobayashi et al., 2006). We confirmed here that only the C-terminal region of h-Prune enhances the cell motility properties. Conversely, the N-terminal construct did not enhance these properties, definitively assigning these functions to the most carboxyl-terminus region of the h-Prune protein.

H-Prune-C419S mutant function (Supplementary Fig. 1g-i, related to Fig. 4)

To confirm a direct correlation of Nm23-H1/ h-Prune complex formation and enhancement of cell motility, we evaluate h-Prune-C419S mutant function on HEK293 cell in two-dimensional cell-migration assay. We observed that the h-Prune-C419S mutant impaired the disulfide bridge and substantially altered the three-dimensional structure of the C-terminal region, and it did not affect cell motility (Supplementary Fig. 1g,h). In support of the previous findings, the chromatography assay presented in Supplementary Fig. 1i shows the protein-protein interactions that occur between Nm23-H1 and the h-Prune-C419S mutant protein.

NMR (Supplementary Fig. 2, related to Fig. 2)

NMR diffusion ordered spectroscopy measurements of the h-Prune C-terminal indicated a protein diffusion coefficient of $0.66 \pm 0.05 \times 10^{-10}$ m^2s^{-1}, which corresponds to a hydrodynamic radius (r_H)

of 3.4 ± 0.2 nm. When combined with light scattering analysis, this r_H provides a molecular mass of 11200 Da ±0.5%, and shows that at millimolar concentrations, the h-Prune C-terminal is a monomer with an elongated conformation.

The ^{1}H NMR spectra [1] of the h-Prune C-terminal are very difficult to assign due to poor dispersion of the resonances. To increase the dispersion of the NMR signals and to allow analysis of the dynamics using multinuclear NMR spectroscopy, uniformly ^{15}N-labeled and $^{15}N/^{13}C$-labeled h-Prune C-terminal samples were prepared. Sequential assignments of the $^{1}H_N$, ^{15}N, ^{13}CO, $^{13}C\alpha$, $^{1}H_\alpha$ and $^{13}C_\beta$ resonances were obtained in full following a standard triple-resonance procedure. A ^{1}H-^{15}N hetero-nuclear single quantum coherence (HSQC) spectrum of the h-Prune C-terminal is shown in Supplementary Fig. S2.

Nuclear Overhauser effects (Supplementary Fig. 3, related to Fig. 2)

These measurements are useful probes of the behaviour of amino acids in intrinsically disordered systems, and they can highlight the relative propensity of different fragments of the primary sequence for local conformations. As shown in Figure 2C, the steady-state heteronuclear ^{1}H-^{15}N NOEs show several changes in sign along the amino-acid sequence. Some regions are characterized by fast motions and high flexibility (negative NOEs) and others are characterized by slower motions. The trends in the NOEs confirm a tendency to adopt transiently folded conformations. In particular, the regions characterized by reduced motion on the nanosecond time scale are amino acids 357-364, 380-386 and 427-440, where a helical secondary structure propensity was indicated by CSI analysis. Other amino-acids with positive NOEs are 418, 419, 422, 423, 424, which highlight another region with reduced motion on the nanosecond time scale, and which are mainly clustered in the disulfide-bridged part of the protein. Analysis of the ^{15}N relaxation rates (R_1 and R_2) establishes that the $\alpha1$ and $\alpha3$ regions (including the disulfide cyclic region), and to a lesser extent the $\alpha2$ helical regions, are characterized by slower conformational behavior, which is very likely due to a more structured conformation.

As expected, the reduced number of sequential connectivities in the [^{1}H, ^{15}N] HSQC-NOESY spectrum confirms the absence of stable elements of the secondary structure. However, some sequential and short-range upper limit constraints were found in the three helical regions, and together with the scalar couplings, these were used for structure calculations. The 20 calculated structures provide compelling evidence that the h-Prune C-terminal molecules represent an "ensemble" of different populations of disordered polypeptide chains, with the exception that the α1, α2 and α3 regions have a helical propensity.

To better understand the Nm23-H1/ h-Prune C-terminal interaction, a series of two-dimensional [^{1}H, ^{15}N]-HSQC experiments were performed. Progressive additions of Nm23-H1 induced line broadening and a strong reduction in the peak intensities of some of the amino acids located in the 387-395 region and in the more compact region constituted by the disulfide-bridged cycle and the α3 helical region (amino acids 410-440). This should therefore represent the Nm23-H1 binding epitope (**Fig. 3a-c and Supplementary Fig. 3a**).

Additionally, as indicated above, we synthesized a specific competitive peptide, CPP (Garzia et al., 2008) mimicking the minimal region of interaction of Nm23-H1 (amino acids 115-128), which is able to bind to the C-terminal of h-Prune. Thus this interaction of CPP with h-Prune C-terminal was also followed via chemical shift mapping. As expected, this chemical shift mapping of the CPP binding site of the h-Prune C-terminal (**Supplementary Fig. 3b**) revealed a small surface that is virtually entirely included in the Nm23-H1 binding region of the h-Prune C-terminal.

Interestingly, the N-terminal region of the h-Prune C-terminal (amino acids 354-369) that the NMR analysis has shown to have mostly helical propensity (a1) is actually part of the last region of the globular DHH2 domain.

The h-Prune interaction with Nm23-H1 is mediated by the IDP domain, particularly through the small globular region and by amino acids 387-396, including the a2 C-terminus (Fig. 3). This suggests that in the Nm23-H1/ C-terminal h-Prune complex, the entropic cost of approaching the

amino acid 387-396 region to the globular region will probably be balanced by the enthalpic contribution of the interaction between Nm23-H1 and the h-Prune C-terminal globular region. Interestingly, the h-Prune C-terminal interaction surface, seen as the smaller CPP, preserves most of the amino acids of the 387-396 region but a much smaller part of the C-terminal globular region.

CPP function validation (Supplementary Fig. 4f, related to Fig. 4)

To further validate the function of the CPP peptide, we assessed this protein region in the presence and absence of the TAT protein region and HA epitopes. Here there was no influence of either epitope (TAT, HA) on the activity of CPP in terms of its biological function, thus strengthening its active function of impairment of NBL.

TRIM22 and PTPRA expression in the SH-SY5Y xenograft tumors (Supplementary Fig. 5c, related to Fig. 6)

An immunohistochemistry analyses was performed to determine the expression of TRIM22 and PTPRA in the SH-SY5Y xenograft tumors. As shown in Figure S5B, the Ad-CPP-treated tumors showed lower positivity for TRIM22 and PTPRA than those of the Ad-Mock tumors, and these results were also confirmed by Western blotting (Fig. 6c). Altogether, these data support the concept that the results obtained *in vitro* can be significantly reproduced *in vivo*. Hence, the use of CPP in those tumors can down-regulate TRIM22 and PTPRA overexpression *in vivo*, as a sign of therapeutic benefit.

CPP effect on tumor microenviroment (Supplementary Fig. 5d,e, related to Fig. 6)

As CPP reduces the amount of phospho-Iκb-α (on Ser32/36), we investigated the potential functionality of CPP for the intracellular levels of NF-κB signaling using the NF-κB reporter luciferase promoter. As shown in Supplementary Fig. 5d, Ad-CPP significantly reduced the levels

of luciferase activity compared to Ad-Mock-infected cells ($p = 5.91\ e^{-07}$). Thus, this prompted us to test if the NBL SH-SY5Y cells treated with CPP can impair the chemotactic attraction of J774 macrophages in a 2D migration assay. To performed this assay we used the conditional medium of treated cells as chemoattractant, thus mimicking *in vitro* tumor metastasis niche. Supplementary Fig. 5e shows that CPP can indeed impair the migratory macrophage phenotype, mainly by acting through inhibition of endogenous NF-κB signaling in SH-SY5Y cells.

Nm23-H1 and h-Prune protein expression in NBL tumors (Supplementary Fig. 6)

As the expression of the Nm23-H1 and h-Prune genes correlates to aggressiveness in NBL (see main text), immunohistochemistry was used to stain different tumor tissues classified by NBL pathology INSS stages I, II, III, and IV, in order to analyze the Nm23-H1 and h-Prune protein expression within each tumor. The results show that, during NBL progression, there is an increase in cells positive to Nm23-H1 and h-Prune staining, supporting the concept of Nm23-H1 and h-Prune as markers of aggressive stages in NBL tumorigenesis (Supplementary Fig. 6a). Then, the same immunohistochemical analysis was performed in a multiple tissue array (TMA), generated by the German Cancer Research Centre, containing 64 NBL tumors in duplicate series (Supplementary Table 2). High expression levels of h-Prune were detected in 42 tumors analyzed (>40% positive cells) and were significantly associated with poor prognosis ($p < 0.02$) (Supplementary Fig. 6b). Within 53 tumor cases analyzed, there were 36 cases at stages III-IV and 17 cases at stages I-II. High expression of Nm23-H1 protein was specifically detected in the same tumors and was also correlated to poor survival ($p = 0.039$) (Supplementary Fig. 6c). Similarly the co-staining with both Nm23-H1 and h-Prune was correlated to poor survival, suggesting that the presence of both markers in NBL indicates a worse prognosis. Although promising, these results did not reach statistical significance ($p = 0.08$), mainly because of the relative small number of patients analyzed here (Figure S6D). As shown in Supplementary Fig. 6e, in the Essen database there was a strict

correlation between N-Myc and Nm23-H1 expression, underlining the importance of those proteins in NBL MNA Type 2B tumors.

Nm23-H1 and h-Prune induce cancer progression in an orthotopic Neuroblastoma xenograft animal model of tumorigenesis (Supplementary Fig. 7**)**

We then investigated the functional effects of increased expression of Nm23-H1 and h-Prune on cellular motility in these previously treated NBL cells. We observed that the overexpression of Nm23-H1 in the NBL cell lines, as well as the overexpression of h-Prune, enhanced cell motility *in vitro* (Supplementary Fig. 7a). Orthotopic xenograft mouse models are valuable tools for improving our understanding and control of NBL metastasis, as they readily represent genetic diversity and allow spontaneous metastasis. Intra-adrenal injections are commonly used for establishing the orthotopic mice models, as human NBL frequently originates in the adrenal gland. To understand to what extend the overexpression of h-Prune mimics the *in vitro* tumor biology data, we used this mouse model to determine the *in vivo* cancer progression effects. For this, female SCID mice (5 weeks old) were injected with 2 $x10^6$ SH-SY5Ycells, as either wild-type or those overexpressing Nm23-H1 or h-Prune (11 mice/group). Standard surgical methodologies were applied.

Here, all of the mice that received the SH-SY5Y cells overexpressing h-Prune died before day 40, when all of the other mice were still alive. Survival analysis by log rank and Wilcoxon tests was performed, which shows that the mice engrafted with h-Prune-overexpressing SH-SY5Y cells had a significantly worst disease status, in terms of mean survival time, as compared to the control wild-type cells and Nm23-H1-bearing animals ($p < 0.0001$) (Supplementary Fig. 7b). Of note, at day 29, mice with SH-SY5Y cells overexpressing h-Prune presented not only tumor cells in the left adrenal gland, but also tumor metastatic cells in the right adrenal gland. Furthermore, in the h-Prune mice, several other organs, such as the liver, gut, ovary and uterus, were seen to be affected by several metastatic foci, when compared with the mice receiving wild-type SH-SY5Y cells ($p < 0.04$) (Supplementary Table 3).

In particular, there were specific h-Prune-positive metastases in the lungs, as a sign of the promotion of angio-invasion (data not shown), thus enhancing our hypothesis that in the appropriate environment, h-Prune positively influences not only cell motility properties, but also the angiogenic and invasion properties of these cells. These results will need future studies to address this area of interest, and their functional correlations.

Similarly, the SH-SY5Y cells overexpressing Nm23-H1 showed a metastatic phenotype although with a delayed effect compared to h-Prune-overexpressing cells ($p < 0.06$), suggesting a lower aggressive potential *in vivo* than *in vitro*. Further studies are needed to fully understand this less aggressive phenomenon that was seen *in vivo*, when compared with the results obtained *in vitro* (an example can be seen in the data of cell motility in Supplementary Fig. 7a. Supplementary Table 3 shows the results from the histopathological analysis of the described *in vivo* models, which demonstrate that the mice with h-Prune-overexpressing SH-SY5Y cells metastasized early, when compared to the wild-type SHSY-5Y-cell-bearing mice. Indeed, the mice injected with h-Prune-overexpressing SH-SY5Y cells had several sites of metastases; e.g., in the lungs. These results will need future studies to address this area of interest and the functional correlations.

The use of a stable clone containing several copies of a sequence that can interfere with the h-Prune mRNA expression (SH-SY5Y-sh-Prune, see Experimental Procedures) resulted in therapeutic benefit, as showed in the significantly improved survival of the mice implanted with this cell clone (**Supplementary Fig. 7c**). However, as h-Prune is ubiquitously expressed as both gene and protein (see gene expression data in Gene Card database), with its cellular biochemistry and physiological function related to intracellular levels of cAMP and polyphosphates, we expect that the use of gene silencing of h-Prune in therapeutic oncology applications *in vivo* would generate side effects. For this reason, we focused our study on the functional role of CPP and its therapeutic applications.

CPP overexpression and h-Prune silencing influence the cell cycle and apoptosis (Supplementary Fig. 8)

To decipher the suppressive mechanisms of CPP overexpression and h-Prune silencing in SH-SY5Yand SK-N-BE cells, we monitored the changes in cell-cycle distribution by fluorescence-activated cell sorting (FACS) analyses. The CPP overexpression and h-Prune silencing resulted in higher fractions of cells in G2 phase at 72 h after infection, compared to the control cells (Supplementary Fig. 8a,b). In order to investigate whether the increase in G2 phase would affect the dynamic of cell growth/proliferation, we used a MTS (3-(4,5-dimethylthiazol-2-yl)-5-(3-carboxymethoxyphenyl)-2-(4-sulfophenyl)-2H-terazolium) assay to measure the viability or cell proliferation for 48h of the NBL cell lines previously infected with Ad-CPP or Ad-sh-Prune. No statistically significant difference was observed in the proliferation between the analyzed samples, as shown in Supplementary Fig. 8c. The same results were obtained in MDA-MB-231 (breast cancer cell line) and PC3 (prostate cancer cell line) cells, while DAOY medulloblastoma cells showed decreasead proliferation at 48 h after CPP overexpression (Supplementary Fig. 8f). We also analyzed the perturbation of apoptosis arising from CPP overexpression, using an Annexin V assay. As shown in Supplementary Fig. 8d, CPP increased the percentage of apoptotic cells, as compared to Ad-Mock infected cells. We also investigated the effects of CPP on caspase activation through measuring caspases 3 activity. Here we observed that the overexpression of CPP or the down-regulation of h-Prune in NBL cells resulted in a significant increase in caspase 3 activity (Supplementary Fig. 8e). No caspase 3 activation was seen in the treated HEK293 cells.

Supplemental Figure Legends

Figure S1. Increased cell motility induced by h-Prune overexpression

(**a**) Two-dimensional migration assay in HEK293 and SH-SY5Y cells showing that overexpression of full-length or C-terminal h-Prune increases cell motility compared to the empty vector control and the N-terminal transfected cells. HEK293 (**b**) and SH-SY5Y (**d**) cells were stably transfetcted

with h-Prune full length (F.L.), h-Prune C-terminal (C.T.), or h-Prune N-terminal (N.T.). Empty vector (E.V.) was used as the control. The cells were stretched and the migrated cells were visualized in the wound the 12 h later. The efficiency of transfection was assessed by Western blotting with an anti-Flag antibody (**c, e**). (**f**) Western blotting to detect the expression of the fusion protein using anti-FLAG monoclonal antibody (data presented in Figure 4D). (**g**) Two-dimensional migration assay in HEK293 cells transfected with the h-Prune full-length mutant (C419S). Data are presented as relative (fold) increases in the number of cells migrating compared with h-Prune full-length wild-type transfected cells. H-Prune full length wild-type cell overexpression significantly increased the migration properties of the cells compared to the empty vector ($p = 0.0019$). No significant reduction in the migration abilities of the cells was seen if they were transfected with mutant C419S compared to wild-type ($p = 0.17$). (**h**) Western blotting analysis was performed to define the expression of the fusion protein using an anti-FLAG monoclonal antibody. (**i**) Affinity chromatography showing that the h-Prune C-terminal protein (C419S) still interacts with Nm23-H1.

Figure S2. Two dimensional ^{1}H-^{15}N HSQC spectrum of the h-Prune C-terminal

(**a**) Backbone amide proton resonances are narrowly dispersed over the range of 7.8 ppm to 8.8 ppm, which is characteristic of unstructured proteins. (**b**) Expanded region to allow labeling of the crowded central region of the spectrum.

Figure S3. NMR relaxation measurements of the h-Prune C-terminal, and NMR mapping studies of the Nm23-H1 binding site on the h-Prune C-terminal

(**a**) Longitudinal relaxation times, R_1, and (**b**) transverse relaxation times, R_2, measured at 600 MHz field strength and plotted against residue number. (**c, d**) Intensity (upper) and chemical shift (lower) variations of the Prune C-terminal ^{1}H-^{15}N HSQC spectra after addition of Nm23H1 (upper) and the CPP peptide (lower), respectively. Cyan shading marks the regions showing large variations upon complexing between Nm23-H1 and the h-Prune C-terminal, and between the h-Prune C-terminal

and the CPP peptide. The magenta shading highlights the regions recognized exclusively by Nm23-H1.

Figure S4. CPP expression and functional validation

(**a**) The competitive permeable peptide (CPP) corresponding to peptides 115–128 within the Nm23-H1 protein sequence containing the region that binds to h-Prune was cloned into an adenoviral vector (Ad) in-frame-fused to the TAT HIV protein sequence. (**b**) CPP mRNA expression detected by RT-PCR in the SH-SY5Y infected cells. (**c**) CPP protein expression evaluated by immunofluorescence assay using an antibody against Ha. (**d**) RT-PCR showing the mRNA expression levels for Nm23-H1 and h-Prune in SH-SY5Y upon CPP treatment. Data are represented as multiples of 2-DCT values compared with Ad-Mock infected cells. (**e**) Upon Ad-CPP and Ad-Mock infections in SK-N-BE, MDA 231T, PC3 and DAOY cells, the protein levels of phosphorylated Nm23-H1, Nm23-H1 and h-Prune were detected by Western blotting. Anti β-actin was used as the loading control. (**f**) To validate the effects of CPP and to ensure that the effects of CPP were not due to the Tat sequence, a 2D migration assay was performed in SH-SY5Y cells transfected with CPP without the Tat sequence, CPP fused with the Tat sequence, and an empty vector as control. Data are represented as means of a number of migrated cells/ field ±standard deviation. (**g**) Invasion of SH-SY5Y cells into Matrigel in a 3D invasion assay. Data are represented as means of number of migrated cells/ field ±standard deviation. CPP ovexpression significantly reduced the invasion properties of SH-SY5Y cells compared to control cells (Ad-V Mock) ($p = 0.00047$).

Figure S5. CPP effects on mRNA expression levels of Nm23-H1 connected genes (Related to Figure 6)

(**a**) mRNA expression levels of Nm23-H1 connected genes in Ad-CPP-infected SH-SY5Ycells, determined by Q-RT-PCR. The levels of mRNA expression were represented as multiples of 2-

DCT values compared with Ad-Mock-infected cells. (**b**) Expression levels of TRIM22 (upper) and PTPRA (lower) were correlated with bad clinical outcome in NBL (p = 0.024 and 7.1 $\times 10^{-4}$, respectively). (**c**) Representative images of the immunostaining for TRIM22 and PTPRA of resected tumors. (**d**) HEK293 cells were infected with Ad-Mock and Ad-CPP at 100 MOI. The following day, the cells were transiently cotransfected with the NF-κB reporter plasmid and pRL–CMV. Twenty-four hours post transfection, the NF-κB–derived luciferase activities were measured after normalizing for transfection efficiency against Renilla luciferase activity. Data are represented as percent changes compared to control. (**e**) Representative motility assays for J774 cells treated with conditioned medium from SH-SY5Y cells (as indicated). Data are represented as percentages of change compared to control.

Figure S6. Nm23-H1 and h-Prune expression in NBL samples

(**a**) Immunohistochemistry staining images of the NBL samples. (**b, c**) Tissue-microarray analyses for Nm23-H1 and h-Prune staining. The survival of these two groups was associated with poor survival. (**d**) Combination of expression within the same NBL tissue of both Nm23-H1 and h-Prune, and correlation to overall survival. (**e**) The mRNA expression levels and their correction in several tumor cohorts in the Essen database underline the correlation of amplification copy number of c-myc and high expression levels of Nm23-H1, compared to those with c-myc single copy. This underlines that the amplification copy number of c-myc correlates to high expression of Nm23-H1.

Figure S7. *In vitro* and *in vivo* effects of Nm23-H1 and h-Prune overexpression

(**a**) Invasion assay performed in SH-SY5Ystable clones overexpressing the Nm23-H1 and h-Prune proteins, as compared to use of the empty vector. (**b**) Overall cumulative *(Cum)* survival is seen to be significantly better for the mouse group injected with SH-SY5Y cells overexpressing Nm23-H1 or h-Prune (p = 0.0001). (**c**) Data indicating that overall cumulative *(Cum)* survival is significantly

better for the mouse group injected with SH-SY5Y cells expressing sh-Prune, compared to the wild-type SH-SY5Y and the h-Prune overexpressing cells ($p < 0.0001$).

Figure S8. H-Prune silencing and CPP overexpression influence cell cycle and apoptosis

(**a, b**) Cell cycle analysis using propidium iodide, showing that CPP overexpression (**a**) and h-Prune silencing (**b**) induce increased numbers of cells in G2 phase at 72 h after infection, compared to the control cells. (**c**) Proliferation assay (MTS) of SH-SY5Yand SK-N-BE cells upon CPP overexpression and h-Prune silencing. (**d**) Annexin V assay showing that SH-SY5Ycells overexpressing CPP undergo apoptotic death (25.8%). (**e**) Analysis of caspase-3 activity in HEK293, SH-SY5Y and SK-N-BE cell lines infected with Ad-CPP, Ad-sh-Prune or Ad-Mock. CPP overexpression induces an increase in caspase-3 activity, as judged by fluorimetric caspase assay in both NBL cell lines (P = 6.44181 E-05 and 0.0003, respectively), as compared to the control vector (Ad-Mock) infected cells. H-Prune silencing induces an increase in caspase-3 activity both in the SH-SY5Yand SK-N-BE cells (P = 3.3 E-05 and 6.9 E-05, respectively), as compared to control vector (Ad-Mock) infected cells. HEK293 cells did not show caspase 3 activation. (**f**) Proliferation assay (MTS) of MDA-MB-231, DAOY and PC3 cells upon CPP overexpression.

Figure S9. Nm23-H1 expression in transgenic mice

(a) Positive correlation between h-Prune and Nm23-H1 (r-value=0.760, p-value=3.9e-04, T-value=4.535, degrees of freedom=15) in ALK mutated, MYCN amplified and wild type NBL cell lines (http://r2.amc.nl; Duijkers et al., 2011). **(b)** Nm23-M1 expression in adrenal glands and tumors from ALK^{F1174L}, LIN28B, TH-MYCN and ALK^{F1174L}/TH-MYCN mice (Essen database). **(c)** Action view of NME1, ALK and PTPRA network (green) obtained by using STRING. Modes of action are shown in different colors. Genes highlighted in yellow were further investigated and impaired by CPP.

Supplemental experimental procedures

Cloning, expression and purification of h-Prune constructs

H-Prune fragments, corresponding to amino acids 16-220 (matching the DHHA domain), 222-360 (encompassing residues involved in the DHHA2 domain), and 354-453 (C-terminal region homologous to Cortexillin) were designed from previous bioinformatic analyses and proteolysis experiments [2]. The coding sequences were obtained by restriction digestion with *Nco*I and *Xho*I from pFASTBAC HT A recombinant vectors previously prepared. The fragments were cloned into the pETM11 and pETM20 vectors (Novagen) containing an N-terminal polyHis tag and polyHis-TrxA tag, respectively. Screening of small-scale expression cultures was performed using different strains of *Escherichia coli*, temperatures, IPTG concentrations and induction lengths.

Large scale expression of the h-Prune C-terminal was performed in *E. coli* BL21(DE3)STAR (Invitrogen). The production was induced at 22 °C for 16 h with 0.5 mM IPTG. The cells were harvested by centrifugation (6000 rpm, 15 min, 4 °C), resuspended in buffer containing 50 mM Tris/HCl, pH 8.0, 150 mM NaCl and the complete protease inhibitor cocktail (Roche), and then lysed by sonication. The crude cell extract was clarified by centrifugation at 18000 rpm for 30 min, and the supernatant was applied to a HisTrap affinity chromatography column connected to an AKTA Purifier system (GE-Healthcare) and equilibrated with 50 mM Tris/HCl, pH 8.0, 300 mM NaCl, 10 mM imidazole. Trx-h-Prune C-terminal was eluted with high concentrations of imidazole. The pools of interest were dialyzed overnight against TEV buffer (50 mM Tris/HCl, pH 8.0) at 4 °C. TEV protease was added using a molar ratio (protease: substrate) of 1:50; the cleavage was allowed to proceed 3 h at 30 °C. The mixture was then loaded onto a HisTrap column and purification was performed under the same conditions described above. Size exclusion chromatography was performed as the last step of the purification. The runs were carried out at a flow of 1 ml/min on a Superdex-75 16/60 column, connected to the AKTA Purifier system (GE-

Healthcare), and equilibrated in 50 mM Tris/HCl, pH 8.0, 150 mM NaCl. Molecular weight standards from GE-Healthcare were used to calibrate the column. The pools of interest were concentrated using an Amicon Ultra Centrifugal Filter Device with a cut-off of 3 kDa (Millipore). The purity of the recombinant h-Prune C-terminal was confirmed by SDS-PAGE and was routinely higher than 95%.

Expression of ^{15}N-labeled and ^{15}N/^{13}C-labeled recombinant h-Prune C-terminal for NMR studies

A single clone of the JM101 strain was cultured for 3 h at 37 °C in 5 ml LB medium without antibiotics and then inoculated into M9 medium containing 1 g/l $^{15}NH_4Cl$ or 1 g/l $^{15}NH_4Cl$ and 0.5 g/l $^{13}C_6$-glucose as the sole nitrogen and carbon sources. The cells were grown overnight at 37 °C, harvested and lysed with 37% HCl at 95 °C for 8 h, to obtain a mixture of ^{15}N or ^{15}N/^{13}C labeled amino acids. This mixture was used to enrich M9 medium for the expression of the h-Prune C-terminal in the *E. coli* BL21 (DE3) STAR strain previously transformed with pETM20/prune 354-453 recombinant expression vector. The expression and protein purification were performed as described for the unlabeled protein.

Characterization of h-Prune (354-453)

The prediction of the secondary structures of the h-Prune C-terminal was carried out with different algorithms and programs (GOR(IV), AGADIR, JPred, PredictProtein, NNPredict) that are provided through the Expasy web site. In addition, the disorder prediction program PONDR-Predictor of Natural Disordered Regions (http://www.pondr.com/) was used. Far-UV circular dichroism spectra were obtained using a Jasco J-715 spectropolarimeter equipped with a PTC-423S/15 Peltier temperature controller, in a 0.1 mm quartz cell. Spectra were acquired according to the following parameters: far UV range of 260 nm to 190 nm, band width of 1 nm, response of 8 s, data pitch of 0.2 nm, and scanning speed of 10 nm/min. Conformational studies on the function of pH were

performed by recording spectra at 20 °C, at a protein concentration of 3.5 μM, in the following buffers: 20 mM Na phosphate pH 7.0, 10 mM Tris/HCl pH 8.0 and 9.0, 10 mM Na acetate pH 5.2. TFE-dependent conformational changes were analyzed by adding 5%, 10%, 15%, 20%, 25% and 30% TFE (Sigma-Aldrich) to a 10 μM protein sample in 10 mM Tris/HCl pH 8.0. Spectra processing was obtained using the Spectra Manager software. Light scattering studies were performed using a SEC-LS system that consisted of a semi-preparative size exclusion chromatography column (Superdex-75 10/30, GE-Healthcare) coupled to a miniDAWN™ TREOS triple-angle light scattering detector, and a Shodex RI-101 refractive index detector, supplied by Wyatt Technology Corporation. The run was carried out in 50 mM Tris/HCl, pH 8.0, at a flow rate of 0.5 ml/min.

Protein alkylation and LC-ESI-MS analyses

The h-Prune C-terminal (50 μg) was denatured in 50 μl of a solution containing 250 mM Tris/HCl, pH 8.5, 1.0 mM EDTA, 6 M guanidinium chloride for 30 min at 45 °C, in the absence of any reducing agents. The protein was then subjected to alkylation by incubation of the sample mix in 0.12 M 4-vinyl-pyridine (4-VP) (Sigma-Aldrich) at 25 °C for 60 min, after which time the reaction was terminated by quenching at 4 °C [3]. As a control, after denaturation, the protein was reduced before 4-VP alkylation. Then 0.2 μg of alkylated and control sample were run on LC-ESI-MS analyses, performed as described previously [3].

Limited proteolysis analyses

Limited proteolysis analyses were performed by incubation of 6 μg of purified h-Prune C-terminal together with the selected enzyme in 60 μl of a solution containing 10 mM Tris HCl, pH 8.0/ 10 mM phosphate buffer, pH 7.0, at 4 °C or 22 °C. TPCK-treated trypsin (Sigma-Aldrich) was used at enzyme: substrate ratios of 1:100 and 1:1000, and the resulting peptide mixtures were analysed at 0, 1, 3, 5, 7 and 16 h. In contrast, digestions with GluC (Roche, Penzberg, Germany) were carried out

at U enzyme: U substrate ratios of 0.01:1 and 0.04:1, at 22 °C, according to manifacturer suggestions, monitoring proteolysis at 0, 1, 2, 4, 6 and 16 h. After digestion, the samples were quenched with 5% TFA and stored at -20 °C; 5 mM DTT was added to the samples before the LC-ESI-MS/MS analysis.

Nm23-H1 and CPP protein production

The coding region for CPP was amplified from the construct including the Nm23-H1 region 115-128 amino acids downstream in-frame to the Ha sequence and upstream of the TAT sequence, with the *Nco*I and *Xho*I restriction sites inserted by PCR. Then, the *Nco*I-*Xho*I fragment was introduced into the pETM-11 expression vector (Novagen) with an N-terminal His tag. The Nm23-H1construct was subcloned from pET151 into the pET28(a+) plasmid with an N-terminal His tag. *E. coli* Rosetta-pLysS cells (Invitrogen) were transformed with the sequenced clones. Recombinant cells were grown to an optical density at 600 nm of 0.6 in LB medium supplemented with kanamycin (50 μg/ml) and chloramphenicol (33 μg/ml), at 37 °C. Induction was carried out by the addition of 0.5 mM IPTG to the medium, and the growth was continued at 22 °C overnight. The cells were then harvested by centrifugation, and the cell lysis and affinity purification steps were performed as described above for h-Prune C-terminal, except for the addition of 1 mM DTT to the buffer. The homogeneous recombinant proteins were subjected to phosphorylation with casein kinase gamma (Invitrogen) and used for the different purposes. The phosphorylated samples were concentrated to 0.6 mM and used for NMR studies.

NMR

NMR analyses were performed on a 600 MHz Varian Inova spectrometer (Varian Inc., Palo Alto, CA, USA) equipped with a cold probe. Diffusion-ordered NMR spectroscopy (DOSY) [4] was performed using the Pulsed Gradient Spin-Echo (PSGE) NMR method [5] The following relationships existed between the translational self-diffusion parameter, D, and the NMR

parameters: $I/I_0 = - \exp[D \gamma^2 \delta^2 G^2(\Delta - \delta/3)]$; where I is the measured peak intensity of a particular group of resonances; I_0 is the maximum peak intensity of the same group of resonances at the smaller gradient strength; D is the translational self-diffusion constant (in m^2s^{-1}); γ is the gyromagnetic ratio of a proton (2.675×10^4 rad $G^{-1}s^{-1}$); δ is the duration of the gradient (in s); G is the strength of the gradient (in G cm^{-1}); and Δ is the time between the two gradients (in s). Experiments were acquired by using the longitudinal eddy-current delay (PFG-LED) pulse sequence, with a post gradient eddy-current relaxation of 5 ms. Each experiment was averaged over 128 scans, and the number of points was 16000. The strength of the gradient pulses was varied from 2% of the total power of the gradient coil to 95%, and their shape was a sine function. The duration of the gradient was varied between 3.0 ms and 2.0 ms, and the time between both gradients was changed between 100 ms and 150 ms. The rH was estimated from the Stokes–Einstein equation: $(K_BT) / (6\pi\eta D_t)$, where K_B is the Boltzmann constant, T is the temperature in Kelvin, and η is the viscosity of the solution. All of the backbone assignment experiments of the $^{15}N/^{13}C$-labeled h-Prune C-terminal were carried out at 298 K using data from 2D [^1H-^{15}N] HSQC, 3D HNCO, HN(CA)CO, HNCACB, CBCA(CO)NH and HNHA [6].

The dimensions of the resulting processed datasets were 4096 × 1024 for the 2D [^1H-^{15}N] HSQC, and 2048 × 256 × 128 for all of the 3D experiments.

The pulse sequences used were sensitivity enhanced (with the exception of the HNHA experiment), and used gradients for coherence selection and water suppression [7]. The 3D [^1H-^{15}N] HSQC NOESY and [^1H-^{15}N] HSQC TOCSY were recorded with mixing times of 200 ms and 60 ms, respectively. The spectra were processed using Sparky [8] and assigned using CARA [9]. Random coil values were subtracted from the measured chemical shifts after corrections for sequence effects [10]. Structure calculations, which used the torsion angle dynamics protocol of CYANA software (Hermann et al., 2002) were then started from 100 randomized conformers. The 20 conformers with the lowest CYANA target function were further refined by means of restrained energy minimization, using the Gromos 96 force field, with the program SPDB VIEWER [11]. The color

figures and the structure analysis were performed with the program MOLMOL [12]. NMR relaxation data were collected on ^{15}N-labeled h-Prune C-terminal at a concentration of 0.150 mM. Cross-peak intensities were measured as peak heights. The errors in the relaxation rates were calculated using the signal-to-noise ratios of the individual peaks and the fits of the data to the decays.

Duplicate measurements were carried out to determine the error estimates. The 2D [^{1}H, ^{15}N] HSQC spectra, and the [^{1}H]-^{15}N NOE measurements [13] were acquired with 1024 (HN) × 128 (N) data points, and 16 (for R1 and R2) or 64 (for NOE) scans. R1 values were measured in a series of spectra with relaxation delays of 50, 100, 250, 500, 1000, 1500, 3000 and 4000 ms. R2 measurements were taken with relaxation delays of 30, 60, 90, 120, 150, 180, 210 and 240 ms. The [^{1}H]-^{15}N steady-state NOE values were obtained from ratios of peak heights from experiments with (I_{noe}) and without (I_{nonoe}) saturation of the protons for 5 s at the beginning of the experiments. The heteronuclear NOE values were obtained from ($I_{noe} - I_{nonoe/} I_{nonoe}$).

Protein–protein and protein-peptide interaction studies were conducted using NMR titration experiments and analysis of 2D [^{1}H-^{15}N] HSQC spectra. To identify the h-Prune C-terminal binding interface for Nm23-H1, 2D [^{1}H-^{15}N] HSQC spectra of ^{15}N-labeled h-Prune C-terminal (100 μM) were recorded for the protein in the unbound form and after addition of unlabeled Nm23-H1 (25, 50, 75, 100 μM). To confirm the binding of the h-Prune C-terminal interface to Nm23-H1, NMR chemical shift perturbation experiments were performed with ^{15}N-labeled h-Prune C-terminal samples (100 μM) and unlabeled CPP peptide concentrations ranging from 100 μM to 1 mM.

Homology modeling and molecular dynamics simulations

All calculations and graphical analyses were run on a Silicon Graphics Octene2 workstation. The INSIGHT/DISCOVER program (Accelrys) was used to build the preliminary structure and to perform energy minimizations and molecular dynamics simulations *in vacuo*, pH 7.0, using the CVFF force field (1-3). The 3D model of full length h-Prune was built using the protein homology recognition SWISS-MODEL server [11, 14, 15] and the NMR structure h-Prune C-terminal. SWISS-

MODEL server scored yeast PPX1 [16] (PDB code 2qb7) as the best template, with 21.9% sequence identity on the full-length protein. A careful check of the 3D model that was built was carried out to check for the occurrence of bugs due to insertions and/or deletions within the template secondary structure elements.

The SWISS-MODEL server was able to build residue from 1 to 362. Then, to built the full-length protein, the backbone atoms from 355 to 362 of a representative h-Prune C-terminal NMR structure (355-453) were superimposed with the corresponding residues of a homology model obtained previously. The root mean square deviation (RMSD) of this superimposing was approximately 1.32 Å. Amino acids 355-362 of the homology model were removed, and the two structures were merged. The structural model of the full-length was refined through energy minimization, by 2000 steps of conjugate gradient minimization.

The energy-minimized structure was used as the initial structures for the molecular dynamics simulations *in vacuo* at 300 K. In this simulation, amino acids 1-354 were kept fixed, and only the h-Prune C-terminal domain was able to move.

In all simulations, which were performed with a time step of 1.0 fs, the protein was equilibrated for 300 ps. After this initial step, additional simulations of 800 ps were carried out without rescaling, since the energy was conserved and the average temperature remained essentially constant around the target values. Coordinates and velocities for the four simulations were dumped to a disk every 100 steps during the last 300 ps of simulations. These dumped data were used for the statistical analyses. PDB deposition of the 3D model of full length prune is currently under progress.

Meta-analysis

In order to discover the genes related to Myc activity, and to investigate how these genes might interact, we used a two-stage procedure: we first ranked the genes according to their relatedness to *Myc* expression, and then reconstructed the gene-interaction network for the top ranked genes.

As both c-Myc and n-Myc have roles in the aggressiveness of NBL, we decided to derive a combined indicator (denoted max-Myc) of *Myc* activity by computing their maximum expression. The expression values for the combined indicator were calculated as

$$expr(i, \text{max-Myc}) = \max\{ expr(i, \text{c-Myc}), expr(i, \text{n-Myc}) \}; \quad i = 1 \ldots N \text{ (for all data)},$$

where expr(i,X) is the expression of gene X in sample i.

Using max-Myc, we produced ranked gene lists with the ReliefF algorithm [17]. ReliefF is a machine-learning algorithm for determining the importance of specific features, and we used it here to estimate the strength of the correlation of each gene to the max-Myc activity. ReliefF does not assume independence between the expression levels of different genes, and it has been shown that it can detect important features (in our case, genes) that are not only important independently, but are also important in conjunction.

Our analysis was performed on the publicly available data from two NBL studies: Cologne 2-Color data set with 251 samples [18, 19]. The probes from both of these studies were mapped to Ensembl Transcript IDs. Two ranked lists of probes were produced first, one from each of the two data sets. The two lists were aggregated into a single ranked probe list by computing the means of the individual ranks of each probe. The 50 top ranked probes from the aggregated list were then used for gene-interaction network reconstruction.

Gene expression microarray data provide us with quantitative information on the status of the cell under specific conditions and at a specified time point . Given the availability of large amounts of such data, we can apply engineering techniques to try to reconstruct, or 'reverse-engineer,' interaction networks among genes. There are several reconstruction algorithms, and here we used Aracne [20, 21].

Aracne can reconstruct interaction networks from microarray data. It has favorable computational complexity and can make use of the dynamic range of data (it does not rely on discretization). It also does not make any assumptions on the underlying network structure. The method has been

successfully used for system-wide reconstruction of gene networks in several studies, and in some cases the predictions have also been biochemically validated [20-22]. The strength of interactions between pairs of genes in Aracne is estimated with the mutual information of their expression levels, which measures the mutual dependence of two random variables. Mutual information is symmetric, and the interactions in networks generated by Aracne are thus not directed; i.e., they have no information on whether X influences Y, or *vice versa*. Intuitively, mutual information is similar to correlation; unlike correlation, however, it does not assume a linear relationship between the two variables. Our network was reconstructed from the normalized data from both of the above-mentioned studies [18, 19] taken together, but we only used expression data for the 50 probes that were selected in the first step of the analysis.

The reliability (statistical confidence) of the network built with Aracne can be estimated with bootstrapping. Bootstrapping is a widely used statistical technique, which uses random sampling for assessing variance. In our case, a random sample was drawn from the entire expression dataset, and a network was inferred on this sample. The procedure is then repeated many times, which results in a set of (bootstrap) networks. Now, taking an interaction between two specific genes, we compare its strength in all of the bootstrap networks, and count, if it appears in all bootstrap networks; in this way we can estimate its statistical confidence and improve mutual information estimation. Moreover, all bootstrap networks can be merged into a consensus network, which is more robust to errors in both data and mutual information estimation.

The network presented here was generated in this manner from 100 bootstrap networks. As already mentioned, we used Ensembl Transcript (ENST) IDs for identifying the probes. The networks generated were actually networks with interactions between probes (identified with ENST IDs). Since there can be more than one ENST ID associated to each gene, we next translated each ENST ID to the corresponding gene: As a result, more than one interaction between a given gene pair can appear in a single bootstrap network. Finally, we collected all such interactions from all (100)

bootstrap networks, and counted them. The network presented here only includes interactions that appeared at least 200 times.

PTPRA and TRIM22 correlated genes

To obtain a list of PTPRA- and TRIM22-correlated genes in NBL, we looked through a public database ("R2: microarray analysis and visualization platform (http://r2.amc.nl)"). For PTPRA (prode_id 213795_s_at) we obtained a list of 1962 correlated genes, and for TRIM22 (probe_id 213293_s_at) a list of 2829 genes. Among these, we selected those that had an R value >0.7 or >-0.7 for PTPRA, and those that had an R value >0.8 or >-0.8 for TRIM22. Selected genes for PTPRA and TRIM22 were used to obtain a molecular network from the STRING database, version 9.0 (http://string.embl.de/).

Luciferase assay

To determine the activation state of NF-κB, at 24-h post-infection with the adenovirus (Ad-Mock and Ad-CPP), HEK 293 cells were transfected with the indicated plasmid DNAs (empty vector and h-Prune full-length) together with a pNF-κB-luc construct in six-well plates. 48 hours later, luciferase activity was determined with the luciferase assay system (Promega), according to manufacturer protocol. Renilla luciferase-expressing plasmid was added to the transfection mixture for normalization of the efficiency of transfection.

SH-SY5Y conditioned medium and migration assay

To assess the effects of CPP on cell migration induced by tumor cells, we performed motility assays on J774 cells in the presence of conditioned medium from SH-SY5Y cells infected with Ad-Mock or Ad-CPP, as described above. 500 µl of SH-SY5Y conditioned medium was added into the lower chamber of 8-µm-pore-size Transwell inserts (Corning Incorporated, Costar, Corning, NY, USA) and used as the chemoattractant in the motility assay. To ensure that the migration was due only to

the release of cytokines, the J774 cells were seeded into the upper chamber in DMEM containing the same percentage of fetal bovine serum (10%) as in the lower chamber. The cells were left to migrate for 4 h at 37 °C, and then fixed and counted as described above. Two independent sets of experiments were carried out.

***In vitro* binding assay by affinity chromatography**

Affinity chromatography was performed to check the interaction between h-Prune C-terminal and Nm23-H1. 400 μg of h-Prune C-terminal poly-His-tagged protein were incubated with NI-NTA resin (Qiagen). The resin was previously washed twice in water to remove ethanol, and twice in binding buffer (50 mM Tris HCl, pH 8.0, 300 mM NaCl, 10 mM Imidazole) for equilibration. 500 μg of total protein extract from SH-SY5Y cells previously infected with Ad-Mock or Ad-CPP was then added to the resin and incubated overnight under agitation at 4 °C. The tubes were centrifuged at 4000 rpm for 2 min. The resin was washed in 200 μl elution buffer A (50 mM Tris HCl, pH 8.0, 300 mM NaCl, 20 mM imidazole), and after centrifugation, the resin was washed in 200 μl elution buffer B (50 mM Tris HCl, pH 8.0, 300 mM NaCl, 300 mM imidazole). The collected pools were analyzed by Western blotting and revealed using an anti-Nm23-H1 antibody. The anti-His antibody was used as the control for the tagged protein.

Site-directed mutagenesis

Plasmids containing the full-length (pCS4-3XFlag) and C-terminal-encoding region of h-Prune (pETM11) were used as the template for mutagenesis. Site-directed mutagenesis was performed with QuikChange Lightning site-directed mutagenesis kits (Stratagene, La Jolla, CA, USA), according to the manufacturer protocol. Two overlapping complementary primers containing the desired nucleotide changes were designed for each mutation: D388A, C419S and D422A. Mutations were confirmed by DNA sequencing with an ABI Genetic Analyzer 3730 (Invitrogen Bio Inc., Shanghai, China).

Immunohistochemical analysis in NBL cohorts

14 NBL specimens were formalin fixed and paraffin embedded, and representative sections of each tumour were chosen for morphological and immunohistochemical evaluation. NBL diagnosis, classification, subtyping, staging and other prognostic histopathological features were evaluated according to the International Neuroblastoma Pathology Classification (INPC) and International Neuroblastoma Staging System (INSS). Monoclonal, anti-human, Nm23-H1 (Kamiglia, rabbit polyclonal antibody) and anti-h-Prune (A59) were incubated, and the colorimetric reaction was performed using DAB (Vector, Vector Laboratories, Inc). Microwave pre-treatment was used for Nm23-H1 and h-Prune detection for 15 min at 90 °C in 1 mM EDTA, pH 8. The primary antibody was omitted for negative controls. A multiple tissue array constructed by the German Cancer Research Centre containing almost 62 tumors in duplicate series. This was used in immunohistochemistry analyses using specific antibodies that recognize the human Prune and Nm23-H1 proteins.

Evaluation of TMA results

Tumors were considered positive if at least 10% of the tumour cells were stained. Signal intensity was grouped as follows: Negative (0, expression in <10% of the cells), weakly positive (1,+), moderately positive (2,++) and strongly positive (3,+++). A two-sided Fisher's exact test was used to verify associations among high protein levels of Nm23-H1, h-Prune and the aggressive stage. Nm23-H1 and h-Prune over-expression and its effects on survival were performed according to the Kaplan-Meier method, and the significance of the differences in the survivals was determined using the log-rank test. Three groups were performed to test the influence on survival of the Nm23-H1 and h-Prune additive protein expression: **(-) h-Prune or (-) Nm23-H1**, patients with low protein expression of h-Prune or Nm23-H1; **(+) h-Prune or (+) Nm23-H1**, patients with protein over-expression of h-Prune or Nm23-H1.

Mouse Neuroblastoma xenograft model

The NBL cells were injected in the adrenal glands of mice, as previously reported (Pastorino F. et al., 2003). Briefly, five-week-old female SCID mice purchased from Harlan Laboratories (Harlan Italy-S.Pietro al Natisone, UD), were anesthetized and after laparotomy, they were injected in the capsule of the left adrenal gland with 2 $\times 10^6$ SH-SY5Ycells in 15 μl HEPES buffer (wild-type, PRUNE, sh-PRUNE or NM23H1-transfected) (eleven mice/study group). The lethality of the method was *ca*. 0%. Mice were monitored at least twice weekly for evidence of tumor development, quantification of tumor size, and evidence of tumor-associated morbidity. Histological evaluation of the primary tumors and microscopic metastases was performed for all of tissues at day 29 from cell inoculation. Their organs were fixed in neutral buffered 10% formalin, processed by standard methods, embedded in paraffin, sectioned at 5 μm, and stained with Hematoxylin-Eosin and for immunohistochemistry analysis.

The survival analysis was perfomed according to the Kaplan-Meier method, and the significance of differences in survival were determined using the log-rank test. All of the experiments involving mice have been reviewed and approved by the Licensing and Ethical Committee of the National Cancer Research Institute and by Italian Ministry of Health.

Apoptosis assay

Cells were collected after brief trypsinization, washed once with ice-cold PBS, and subsequently stained with Annexin V and propidium iodide. Stained cells were analyzed by flow cytometry using fluorescence-activated cell sorting analysis.

Caspase-3 activity was measured according to the manufacture protocol (BD Biosciences). Briefly, cell lysates (total protein, 100 μg) were added to reaction mixtures (final volume, 100 μl) containing fluorigenic substrate peptides specific for caspase 3 (DEVD-AFC). The reaction was

performed at 37 °C for 1 h. Fluorescence was measured with a fluorescence microplate reader (excitation wavelength, 400 nm).

Cell viability and cell-cycle assay

Following the CPP treatments, the cells were harvested by brief trypsinization, and then washed twice with ice-cold phosphate-buffered saline. After brief centrifugation, the cell pellets were collected, and approximately 5×10^4 cells were diluted in 20 μg/ml propidium iodide solution, and incubated at 4 °C for 24 h in the dark. The cell-cycle distribution was then analyzed by flow cytometry using fluorescence-activated cell sorting analysis (BD FACS, Canto II, BD Biosciences). The previously SH-SY5Y and SK-N-BE infected cell lines were seeded into 96-well plates at a density of 10^4 cells per well. After 72 h, the metabolic activities of the samples were assessed as a surrogate marker for cell proliferation, using the 3-(4,5-dimethylthiazol-2-yl),5-diphenyltetrazolium bromide (MTT; Sigma) assay, as previously described (de Antonellis et al., 2011). Each value represented six replicates, and each experiment was repeated at least three times.

Immunoflourescence assay

Immunofluorescence staining was conducted with SH-SY5Ycells cultured on cover slips. The cells were fixed in 4% paraformaldehyde and permeabilized for 10 min in phosphate buffer containing 0.1% Triton X-100. The relevant antibodies were then added to a blocking buffer (0.1% Triton X-100, 10% pig serum) at the dilutions recommended by the manufacturers. Laser-scanning confocal microscopy was carried out using an MRC-1024/ES confocal microscope (Bio-Rad, Hercules, USA).

Supplemental References

1. Brodeur, G.M. *et al.* Revisions of the international criteria for neuroblastoma diagnosis, staging, and response to treatment. *Journal of clinical oncology : official journal of the American Society of Clinical Oncology* **11**, 1466-1477 (1993).
2. Middelhaufe, S. *et al.* Domain mapping on the human metastasis regulator protein h-Prune reveals a C-terminal dimerization domain. *The Biochemical journal* **407**, 199-205 (2007).
3. Tornatore, L. *et al.* Gadd45 beta forms a homodimeric complex that binds tightly to MKK7. *Journal of molecular biology* **378**, 97-111 (2008).
4. Morris, K.F. & Johnson, C.S. Diffusion-Ordered 2-Dimensional Nuclear-Magnetic-Resonance Spectroscopy. *J Am Chem Soc* **114**, 3139-3141 (1992).
5. Price, W.S., Hayamizu, K. & Arata, Y. Optimization of the water-PRESS pulse sequence and its integration into pulse sequences for studying biological macromolecules. *Journal of magnetic resonance* **126**, 256-265 (1997).
6. Feher, V.A. *et al.* 1H, 15N, and 13C backbone chemical shift assignments, secondary structure, and magnesium-binding characteristics of the Bacillus subtilis response regulator, Spo0F, determined by heteronuclear high-resolution NMR. *Protein science : a publication of the Protein Society* **4**, 1801-1814 (1995).
7. Farrow, N.A. *et al.* Backbone dynamics of a free and phosphopeptide-complexed Src homology 2 domain studied by 15N NMR relaxation. *Biochemistry* **33**, 5984-6003 (1994).
8. Delaglio, F. *et al.* NMRPipe: a multidimensional spectral processing system based on UNIX pipes. *Journal of biomolecular NMR* **6**, 277-293 (1995).
9. Johnson, B.A. & Blevins, R.A. NMR View: A computer program for the visualization and analysis of NMR data. *Journal of biomolecular NMR* **4**, 603-614 (1994).
10. Schwarzinger, S. *et al.* Sequence-dependent correction of random coil NMR chemical shifts. *J Am Chem Soc* **123**, 2970-2978 (2001).
11. Guex, N. & Peitsch, M.C. SWISS-MODEL and the Swiss-PdbViewer: an environment for comparative protein modeling. *Electrophoresis* **18**, 2714-2723 (1997).

12. Koradi, R., Billeter, M. & Wuthrich, K. MOLMOL: a program for display and analysis of macromolecular structures. *Journal of molecular graphics* **14**, 51-55, 29-32 (1996).

13. Farrow, N.A., Zhang, O., Forman-Kay, J.D. & Kay, L.E. Comparison of the backbone dynamics of a folded and an unfolded SH3 domain existing in equilibrium in aqueous buffer. *Biochemistry* **34**, 868-878 (1995).

14. Arnold, K., Bordoli, L., Kopp, J. & Schwede, T. The SWISS-MODEL workspace: a web-based environment for protein structure homology modelling. *Bioinformatics* **22**, 195-201 (2006).

15. Schwede, T., Kopp, J., Guex, N. & Peitsch, M.C. SWISS-MODEL: An automated protein homology-modeling server. *Nucleic acids research* **31**, 3381-3385 (2003).

16. Ugochukwu, E., Lovering, A.L., Mather, O.C., Young, T.W. & White, S.A. The crystal structure of the cytosolic exopolyphosphatase from Saccharomyces cerevisiae reveals the basis for substrate specificity. *Journal of molecular biology* **371**, 1007-1021 (2007).

17. Robnik-Sikonja, M. & Kononenko, I. Theoretical and empirical analysis of ReliefF and RReliefF. *Mach Learn* **53**, 23-69 (2003).

18. Oberthuer, A. *et al.* Gene-expression based classification of neuroblastoma patients using a customized oligonucleotide-microarray outperforms current clinical risk stratification. *Klin Padiatr* **218**, 192-192 (2006).

19. Schramm, A. *et al.* Prediction of clinical outcome and biological characterization of neuroblastoma by expression profiling. *Oncogene* **24**, 7902-7912 (2005).

20. Margolin, A.A. *et al.* ARACNE: An algorithm for the reconstruction of gene regulatory networks in a mammalian cellular context. *Bmc Bioinformatics* **7** (2006).

21. Margolin, A.A. *et al.* Reverse engineering cellular networks. *Nat Protoc* **1**, 663-672 (2006).

22. Bansal, M., Belcastro, V., Ambesi-Impiombato, A. & di Bernardo, D. How to infer gene networks from expression profiles. *Mol Syst Biol* **3** (2007).

Supplementary Table 1. BLI levels following injections of SH-SY5Y-Luc Ad-Mock and Ad-CPP cells into the left supra surrenal gland of athymic nude mice.

	Ad-Mock				
	DAY0	**WEEK1**	**WEEK2**	**WEEK3**	**WEEK4**
Animal Number					
#1	4.25 E+06	2.51 E+05	2.84 E+05	8.32 E+05	8.33 E+05
#2	5.28 E+06	3.80 E+05	4.15 E+05	1.85 E+06	1.27 E+06
#3	6.65 E+06	3.15 E+05	3.72 E+05	1.62 E+06	1.31 E+06
#4	3.73 E+06	3.05 E+04	6.25 E+05	2.65 E+06	4.95 E+06
#5	1.56 E+06	2.49 E+05	6.78 E+05	7.67 E+05	9.93 E+05
#6	6.62 E+05	2.37 E+05	5.77 E+05	9.73 E+05	5.80 E+06
#7	1.05 E+06	1.11 E+05	4.15 E+05	6.63 E+05	1.06 E+06
	Ad-CPP				
#8	2.22 E+07	3.63 E+05	4.32 E+05	2.62 E+05	2.72 E+05
#9	1.96 E+05	1.57 E+05	4.97 E+04	2.47 E+05	1.10 E+06
#10	2.84 E+06	1.29 E+06	1.26 E+06	1.92 E+06	1.47 E+05
#11	3.38 E+06	1.05 E+06	5.55 E+05	5.15 E+05	7.40 E+05
#12	1.21 E+05	1.66 E+05	1.23 E+05	1.21 E+05	2.38 E+05
#13	1.26 E+06	3.94 E+05	6.44 E+05	4.96 E+05	8.48 E+05
#14	1.21 E+05	3.09 E+05	2.02 E+05	3.04 E+05	5.35 E+05

Supplementary Table 2. Characteristics of the patients.

Variable	n
Geographic origin	65
German	45
Swiss	9
Italian	11
Gender	64
Male	34
Female	30
Stage	64
Low (1-2-5)	37
High(3-4)	27
NMYC copy numbers	57
1	37
>2	20
Survival time	54
Alive = 0	49
Dead =1	13

Supplementary Table 3

Histopathological analyses (29 days)

Tissue	**A1**	**A2**	**A3**	**B1**	**B2**	**B3**	**C1**	**C2**	**C3**
Heart	-	-	-	-	-	-	-	-	-
Brain	-	-	-	-	-	-	-	-	-
Bladder	-	-	-	-	-	-	-	-	-
Humerus	-	-	-	-	-	-	-	-	-
Breast bone	-	-	-	-	-	-	-	-	-
Femur	-	-	-	-	-	-	-	-	-
Vertebral column	-	-	-	-	-	-	-	-	-
Spleen	-	1+ *	-	-	1+ *	1+ *	2+ *	**1+ ***	-
Liver	-	-	-	3+ **	**1+**	1+ **	-	-	-
Kidney right	-	1+ *	-	3+ *	**1+ ***	**3+ ***	1+ *	-	-
Kidney left	1+ *	1+ *	1+ *	**3+ ***	**2+ ***	**3+ ** **	**1+ ** **	**1+ ***	**3+ ***
Adrenal gland right	-	-	-	3+ *	no tissue	1+ *	-	-	-
Adrenal gland left	-	-	-	**3+ ***	**3+ ***	**3+ ** **	**1+ ** **	**1+ ***	no tissue
Lung	-	-	-	-	-	-	-	-	-
Esophagus and stomach	2+ *	1+ *	1+ *	**3+ ***	**2+ ***	**1+ ***	3+ *	1+*	-
Ovaries and tube	-	-	-	-	no tissue	**3+ ***	-	1+ *	1+ *
Uterus	-	-	-	-	-	**3+ ***	-	-	-
Gut (duodenum/ ileum)	-	-	-	3+ *	-	-	-	-	-

1+= 1-3 aggregated cancer cells
2+= 3-5 aggregated cancer cells
3+= > 5 aggregated cancer cells
*= cancer cell localization peritoneal or pericapsular
** = invasive localization of aggregated cancer cells

bold number = aggregate cancer cells ≥ 0.1 cm

(A1, A2, A3) Mice injected with wild-type SH-SY5Y cells; **(B1, B2, B3**) Mice injected with h-Prune-overexpressing SH-SY5Y cells; **(C1, C2, C3**) Mice injected with Nm23-H1-overexpressing SH-SY5Y cells

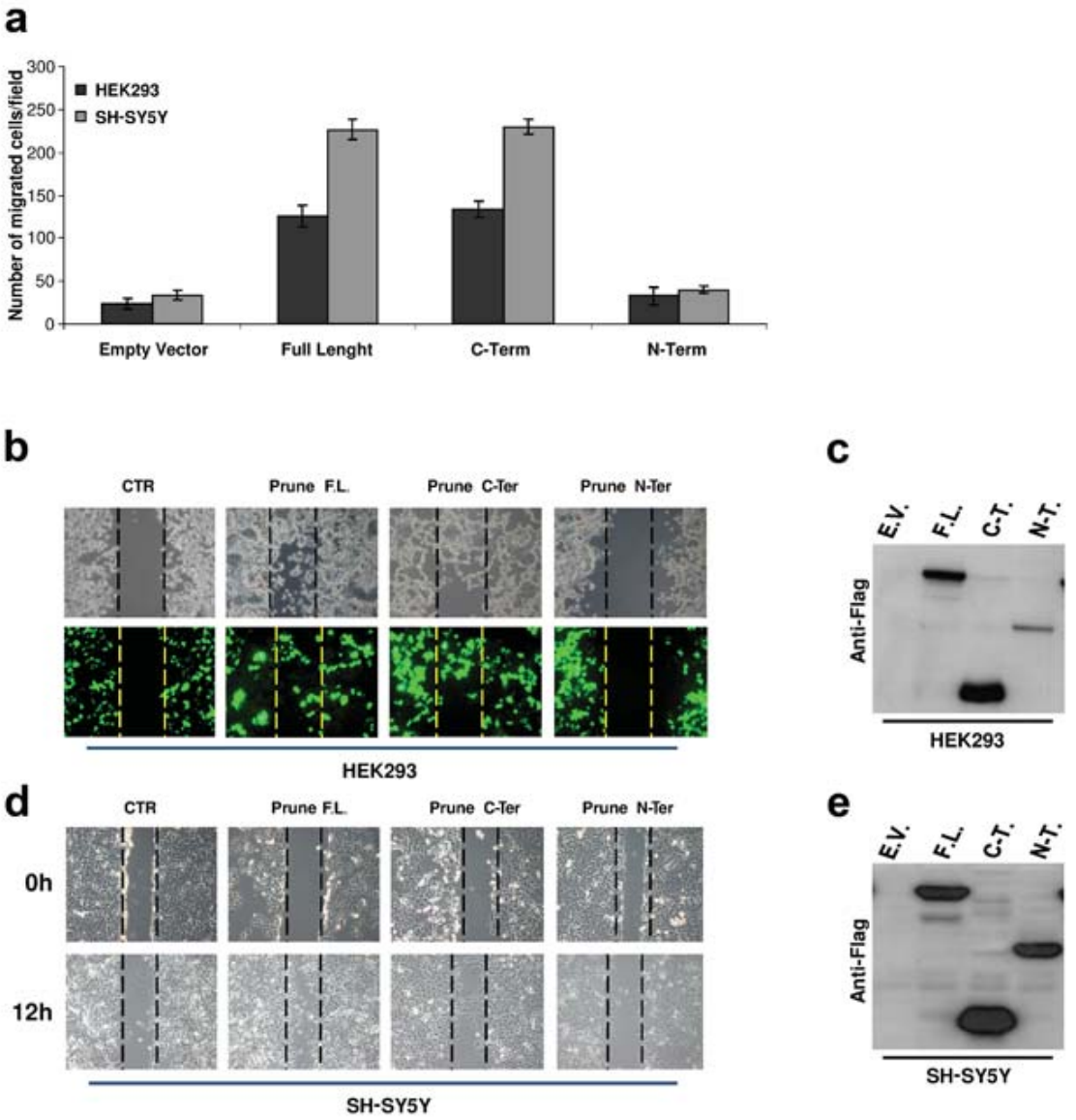
a
Number of migrated cells/field
HEK293
SH-SY5Y
Empty Vector
Full Lenght
C-Term
N-Term
b
CTR
Prune F.L.
Prune C-Ter
Prune N-Ter
HEK293
c
E.V.
F.L.
C.T.
N.T.
Anti-Flag
HEK293
d
0h
12h
SH-SY5Y
e
SH-SY5Y
f
E.V.
W.T
D388A
D422A
Flag
α-Tubulin
h-Prune
g
p-value 0.0019
p-value 0.17
Number of migrated cells (Fold on h-Prune)
CTR
h-Prune
h-Prune C419S
h
CTR
WT
C419S
Flag
α-Tubulin
h-Prune
i
His Prune
SH-SY5Y
E3
E2
E1
Nm23-H1
His Tag
C419S

Figure S1

a

C-Terminal Prune/Nm23-H1

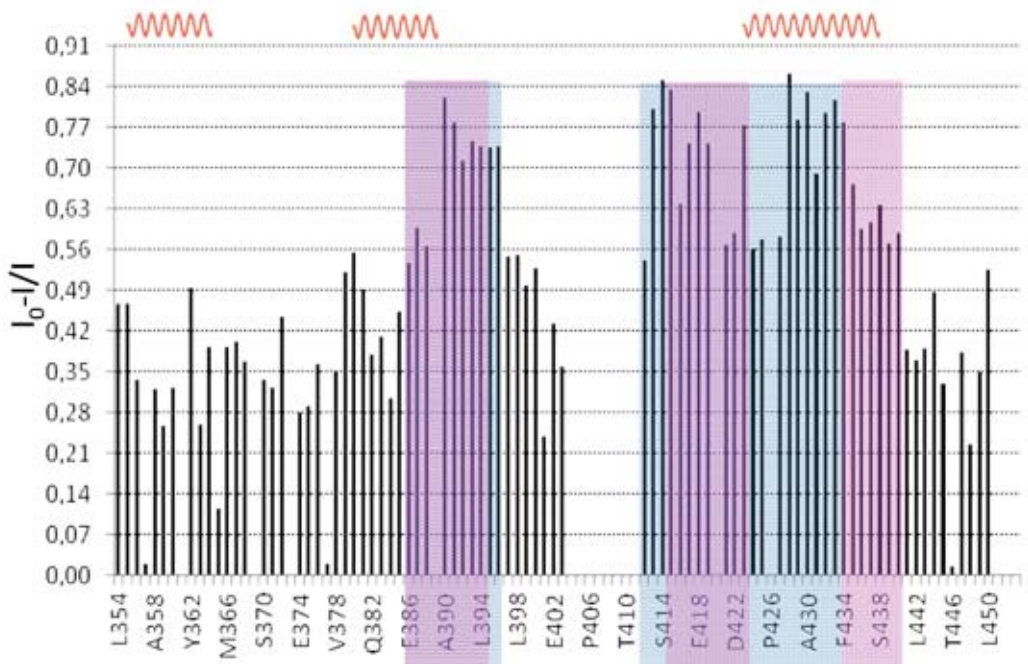

b

C-Terminal Prune/CPP

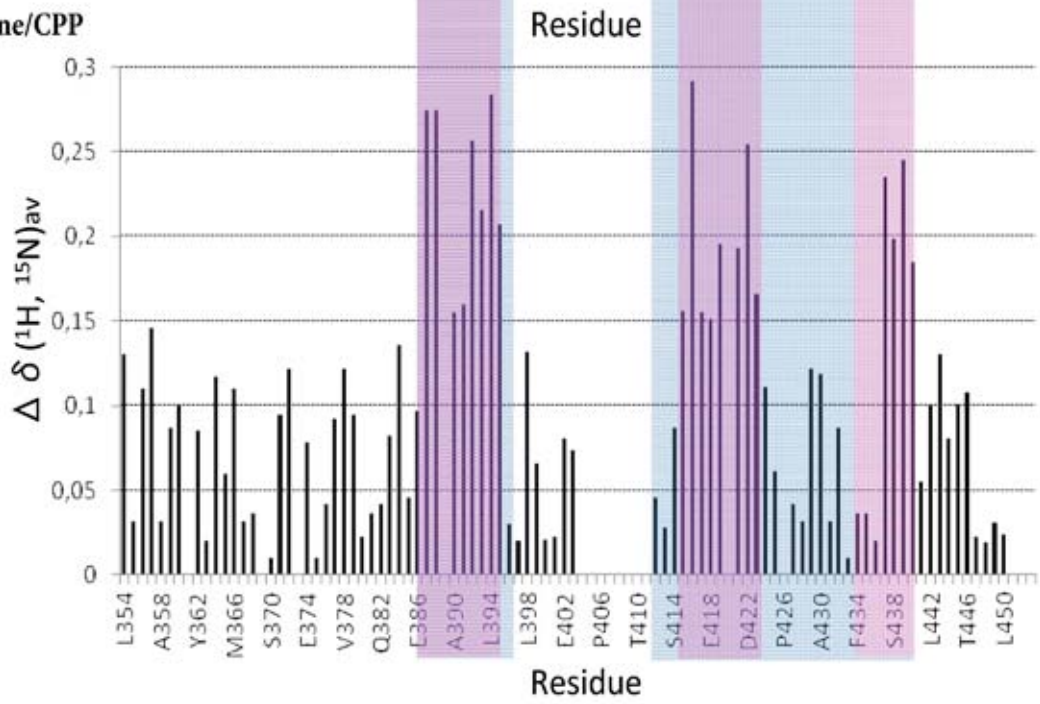

Figure S2

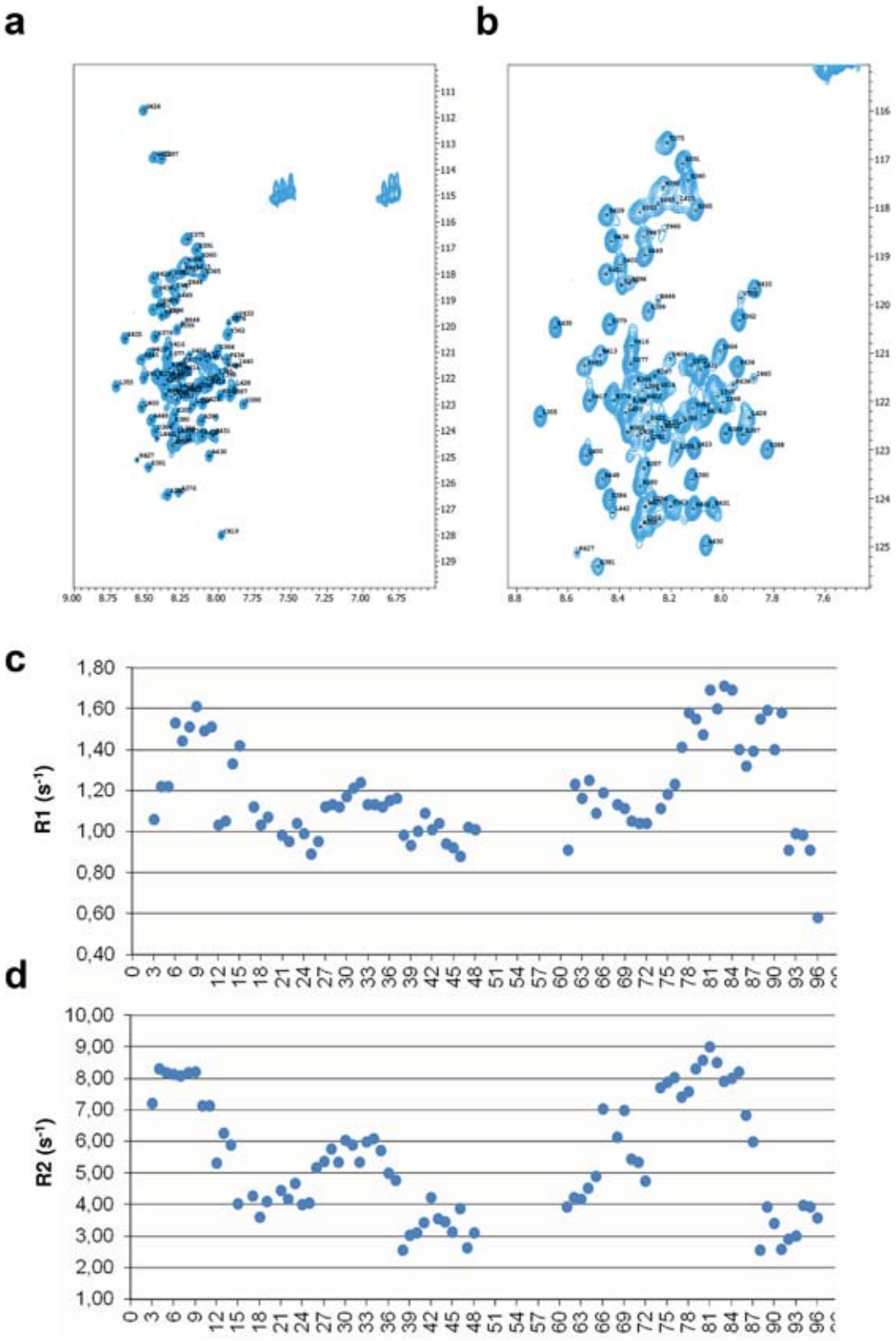

Figure S3

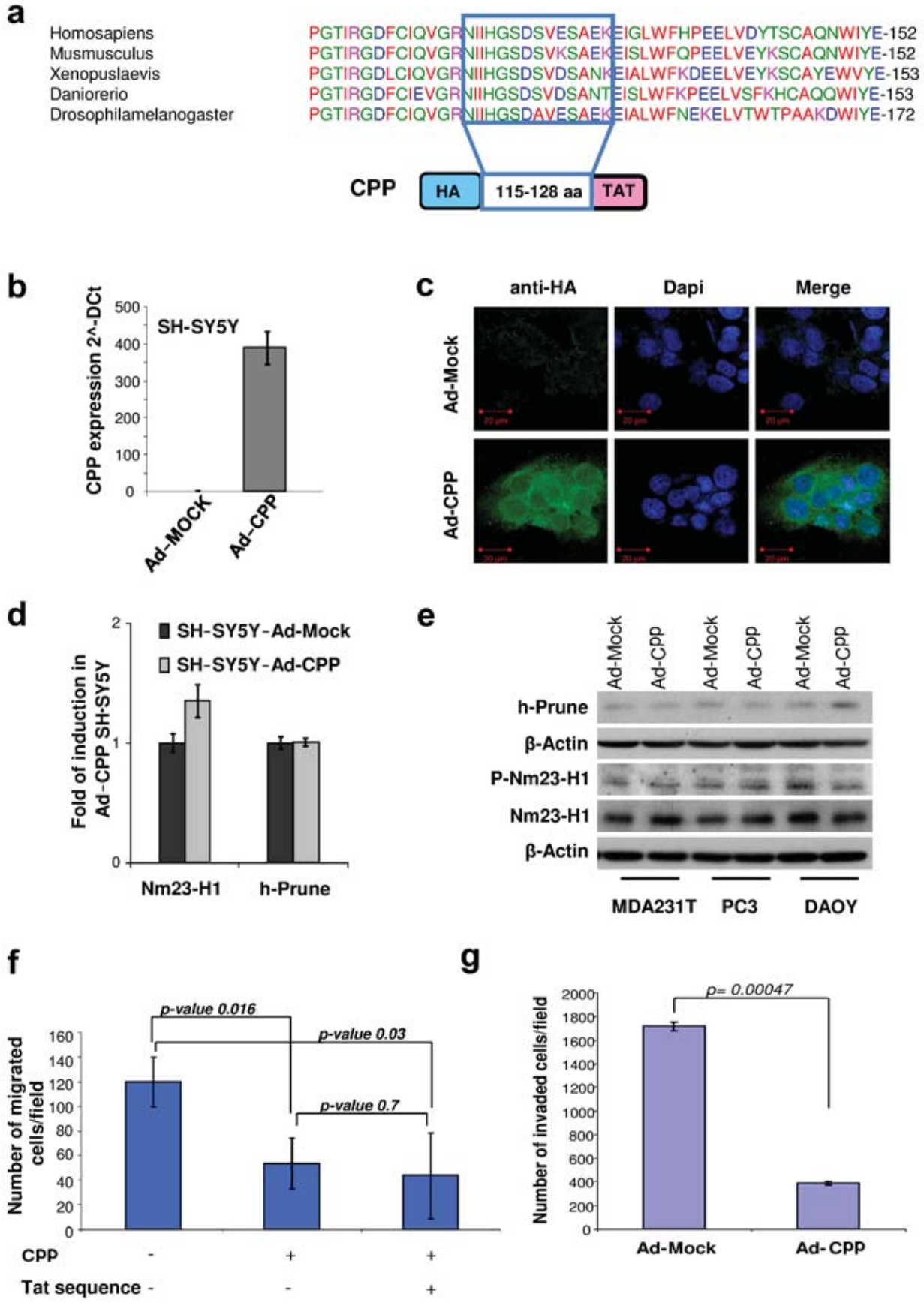
a
Homosapiens PGTIRGDFCIQVGRNIIHGSDSVESAEKEIGLWFHPEELVDYTSCAQNWIYE-152
Musmusculus PGTIRGDFCIQVGRNIIHGSDSVKSAEKEISLWFQPEELVEYKSCAQNWIYE-152
Xenopuslaevis PGTIRGDLCIQVGRNIIHGSDSVDSANKEIALWFKDEELVEYKSCAYEWVYE-153
Daniorerio PGTIRGDFCIEVGRNIIHGSDSVDSANTEISLWFKPEELVSFKHCAQQWIYE-153
Drosophilamelanogaster PGTIRGDFCIQVGRNIIHGSDAVESAEKEIALWFNEKELVTWTPAAKDWIYE-172
CPP
HA
115-128 aa
TAT
b
CPP expression 2^-DCt
SH-SY5Y
Ad-MOCK
Ad-CPP
c
anti-HA
Dapi
Merge
Ad-Mock
Ad-CPP
d
Fold of induction in Ad-CPP SH-SY5Y
SH-SY5Y-Ad-Mock
SH-SY5Y-Ad-CPP
Nm23-H1
h-Prune
e
Ad-Mock
Ad-Cpp
h-Prune
β-Actin
P-Nm23-H1
Nm23-H1
β-Actin
MDA231T
PC3
DAOY
f
Number of migrated cells/field
p-value 0.016
p-value 0.03
p-value 0.7
CPP
Tat sequence
g
Number of invaded cells/field
p= 0.00047
Ad-Mock
Ad-CPP

Figure S4

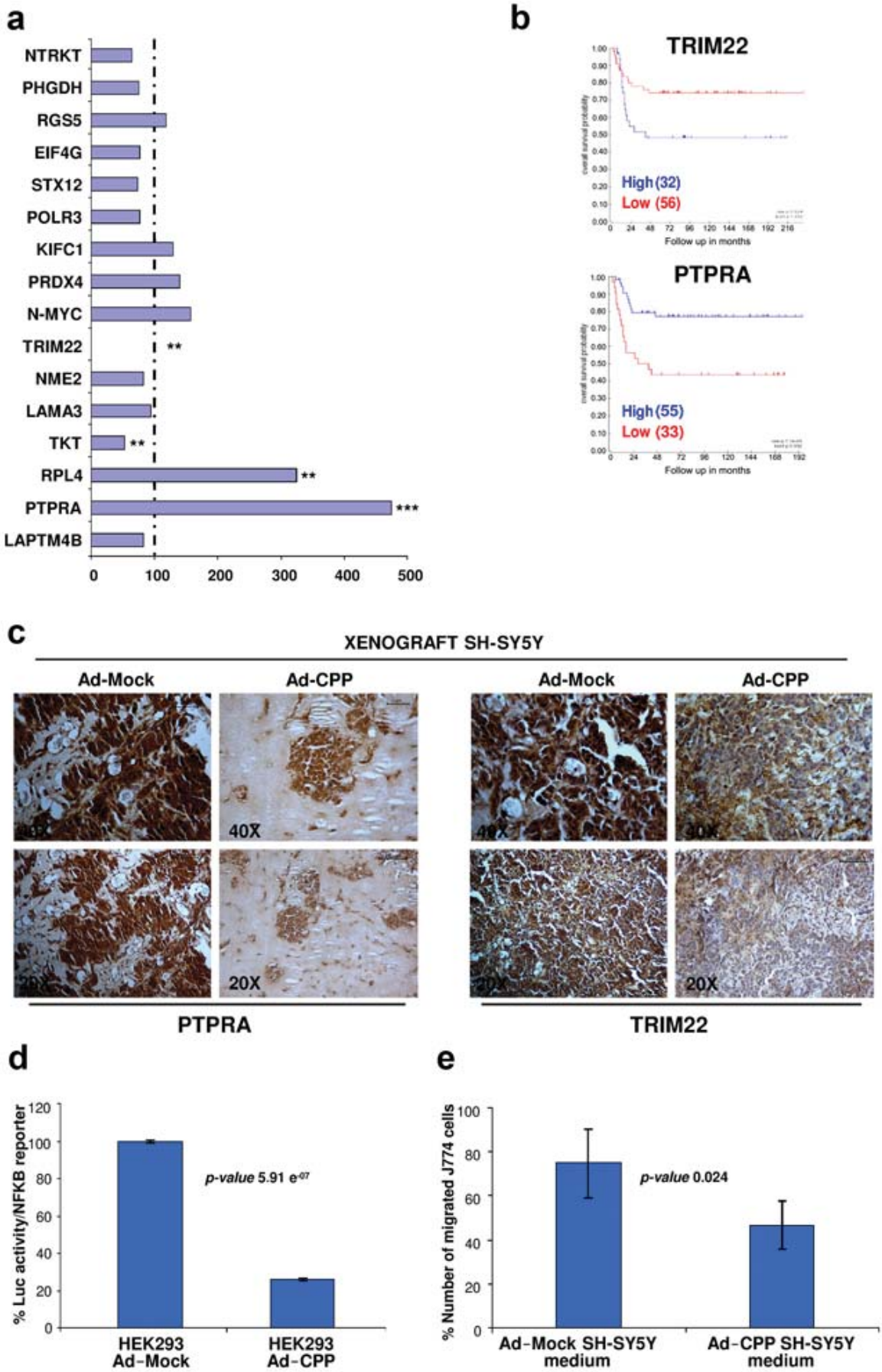
a
NTRKT
PHGDH
RGS5
EIF4G
STX12
POLR3
KIFC1
PRDX4
N-MYC
TRIM22
NME2
LAMA3
TKT
RPL4
PTPRA
LAPTM4B
**
**
***
0
100
200
300
400
500
b
TRIM22
High (32)
Low (56)
Follow up in months
PTPRA
High (55)
Low (33)
Follow up in months
c
XENOGRAFT SH-SY5Y
Ad-Mock
Ad-CPP
Ad-Mock
Ad-CPP
40X
20X
PTPRA
TRIM22
d
% Luc activity/NFKB reporter
p-value 5.91 e-07
HEK293 Ad-Mock
HEK293 Ad-CPP
e
% Number of migrated J774 cells
p-value 0.024
Ad-Mock SH-SY5Y medium
Ad-CPP SH-SY5Y medium

Figure S5

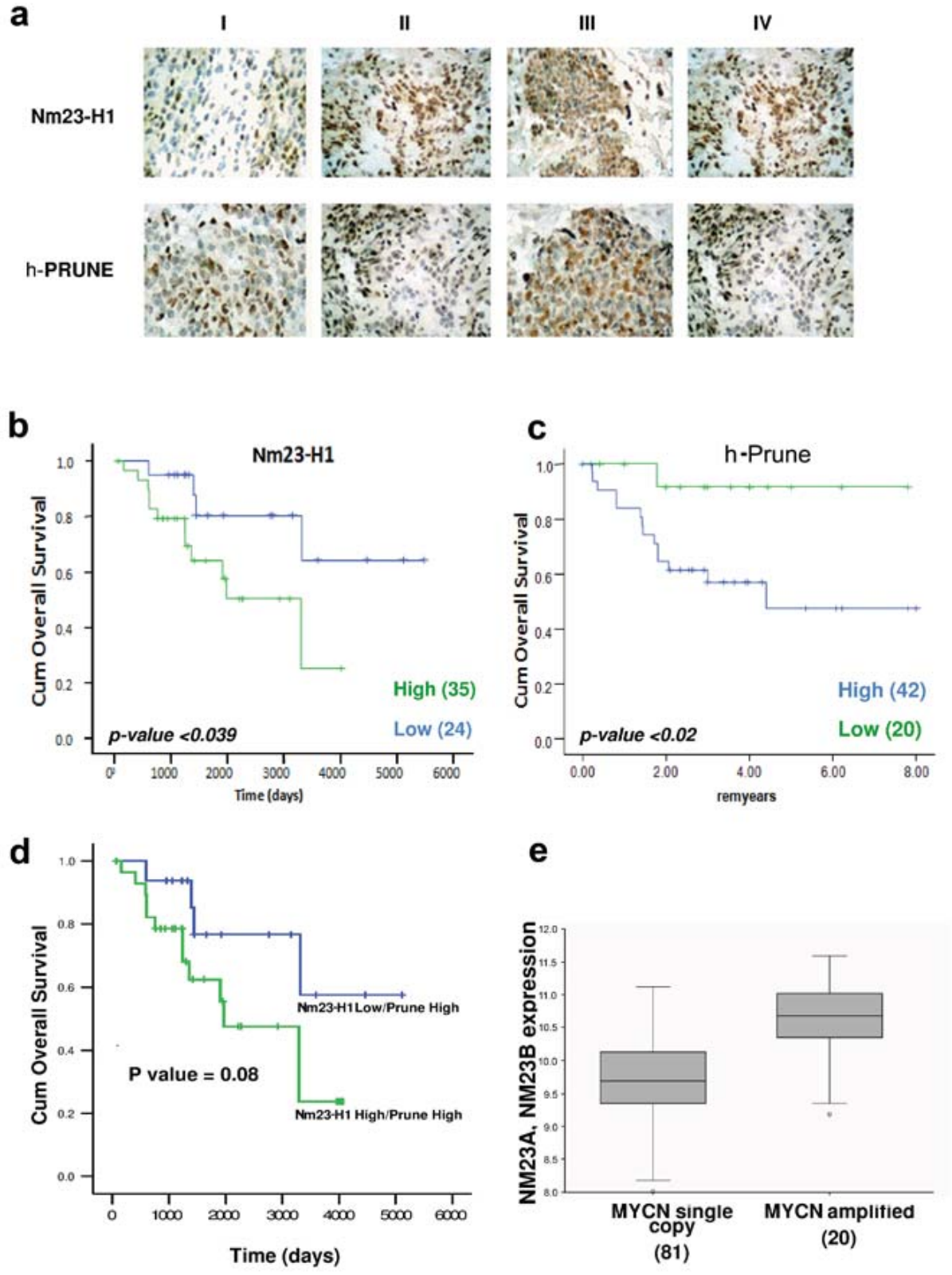
a
I
II
III
IV
Nm23-H1
h-PRUNE
b
Nm23-H1
Cum Overall Survival
High (35)
Low (24)
p-value <0.039
Time (days)
c
h-Prune
Cum Overall Survival
High (42)
Low (20)
p-value <0.02
remyears
d
Cum Overall Survival
Nm23-H1Low/Prune High
P value = 0.08
Nm23-H1 High/Prune High
Time (days)
e
NM23A, NM23B expression
MYCN single copy (81)
MYCN amplified (20)

Figure S6

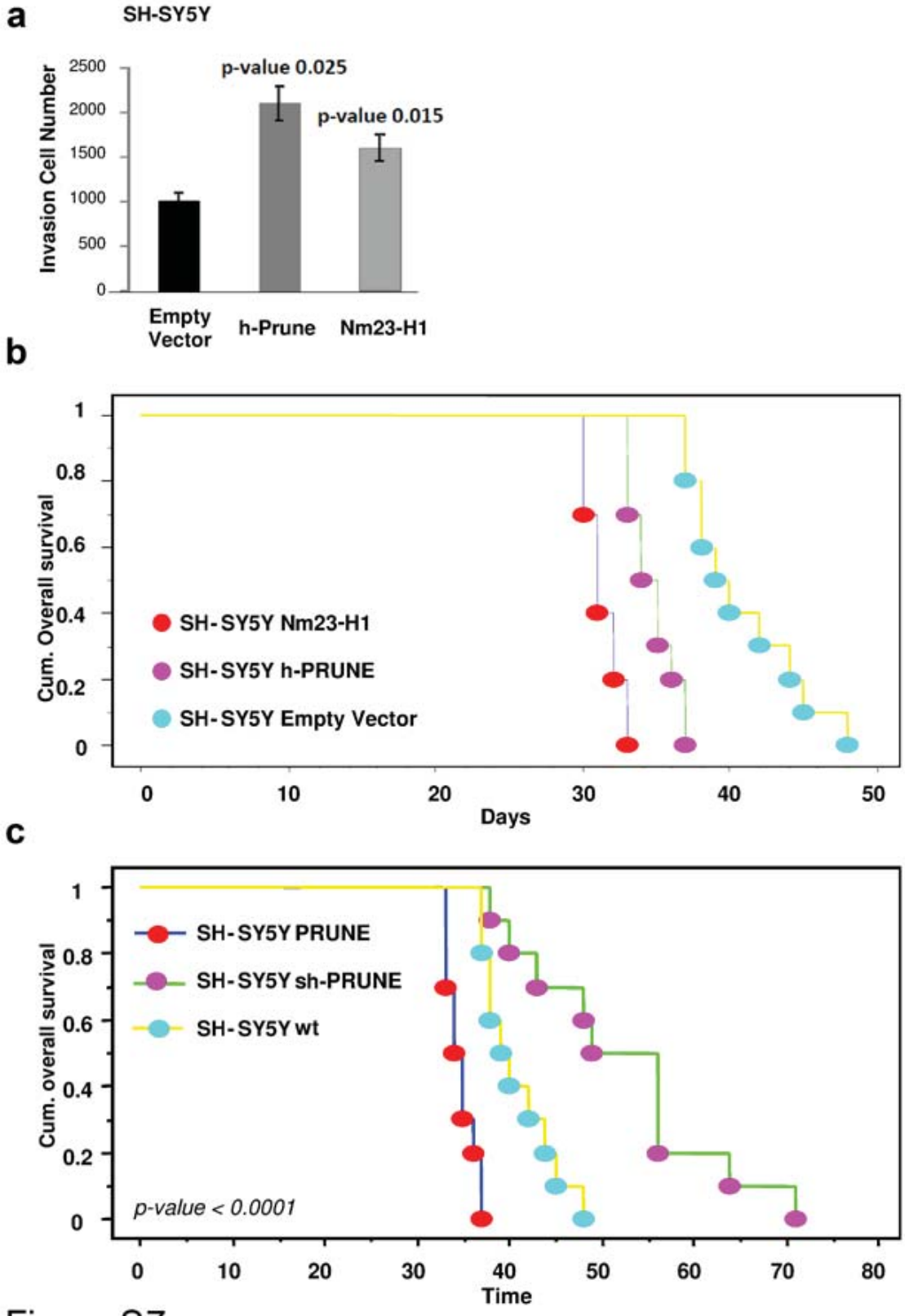
a
SH-SY5Y
Invasion Cell Number
2500
2000
1500
1000
500
0
p-value 0.025
p-value 0.015
Empty Vector
h-Prune
Nm23-H1
b
Cum. Overall survival
1
0.8
0.6
0.4
0.2
0
SH-SY5Y Nm23-H1
SH-SY5Y h-PRUNE
SH-SY5Y Empty Vector
0
10
20
30
40
50
Days
c
Cum. overall survival
1
0.8
0.6
0.4
0.2
0
SH-SY5Y PRUNE
SH-SY5Y sh-PRUNE
SH-SY5Y wt
p-value < 0.0001
0
10
20
30
40
50
60
70
80
Time

Figure S7

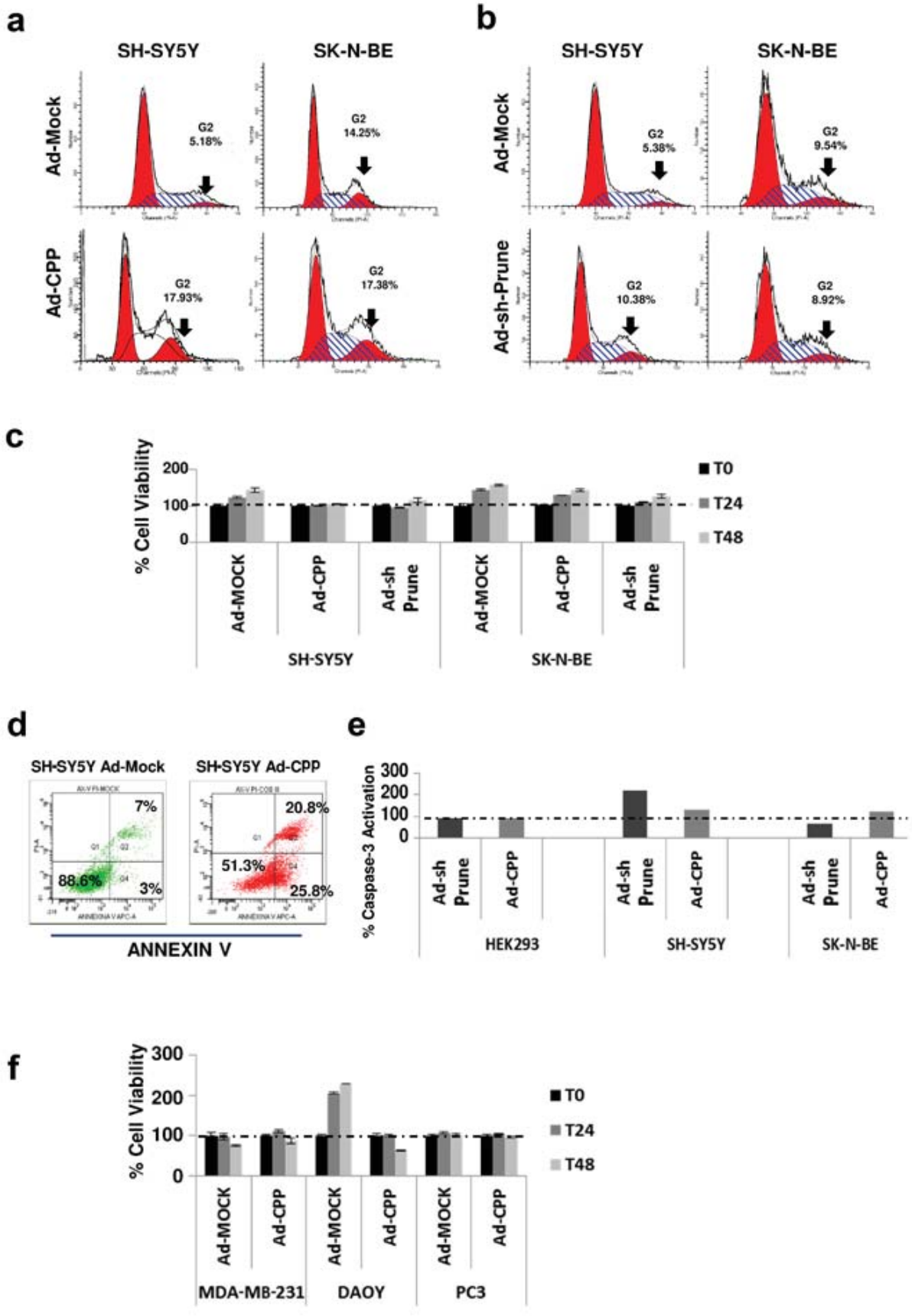
a
SH-SY5Y
SK-N-BE
Ad-Mock
Ad-CPP
G2
5.18%
G2
14.25%
G2
17.93%
G2
17.38%
b
SH-SY5Y
SK-N-BE
Ad-Mock
Ad-sh-Prune
G2
5.38%
G2
9.54%
G2
10.38%
G2
8.92%
c
% Cell Viability
200
100
0
T0
T24
T48
Ad-MOCK
Ad-CPP
Ad-sh Prune
Ad-MOCK
Ad-CPP
Ad-sh Prune
SH-SY5Y
SK-N-BE
d
SH-SY5Y Ad-Mock
SH-SY5Y Ad-CPP
7%
3%
88.6%
20.8%
51.3%
25.8%
ANNEXIN V
e
% Caspase-3 Activation
300
200
100
0
Ad-sh Prune
Ad-CPP
Ad-sh Prune
Ad-CPP
Ad-sh Prune
Ad-CPP
HEK293
SH-SY5Y
SK-N-BE
f
% Cell Viability
300
200
100
0
T0
T24
T48
Ad-MOCK
Ad-CPP
Ad-MOCK
Ad-CPP
Ad-MOCK
Ad-CPP
MDA-MB-231
DAOY
PC3

Figure S8

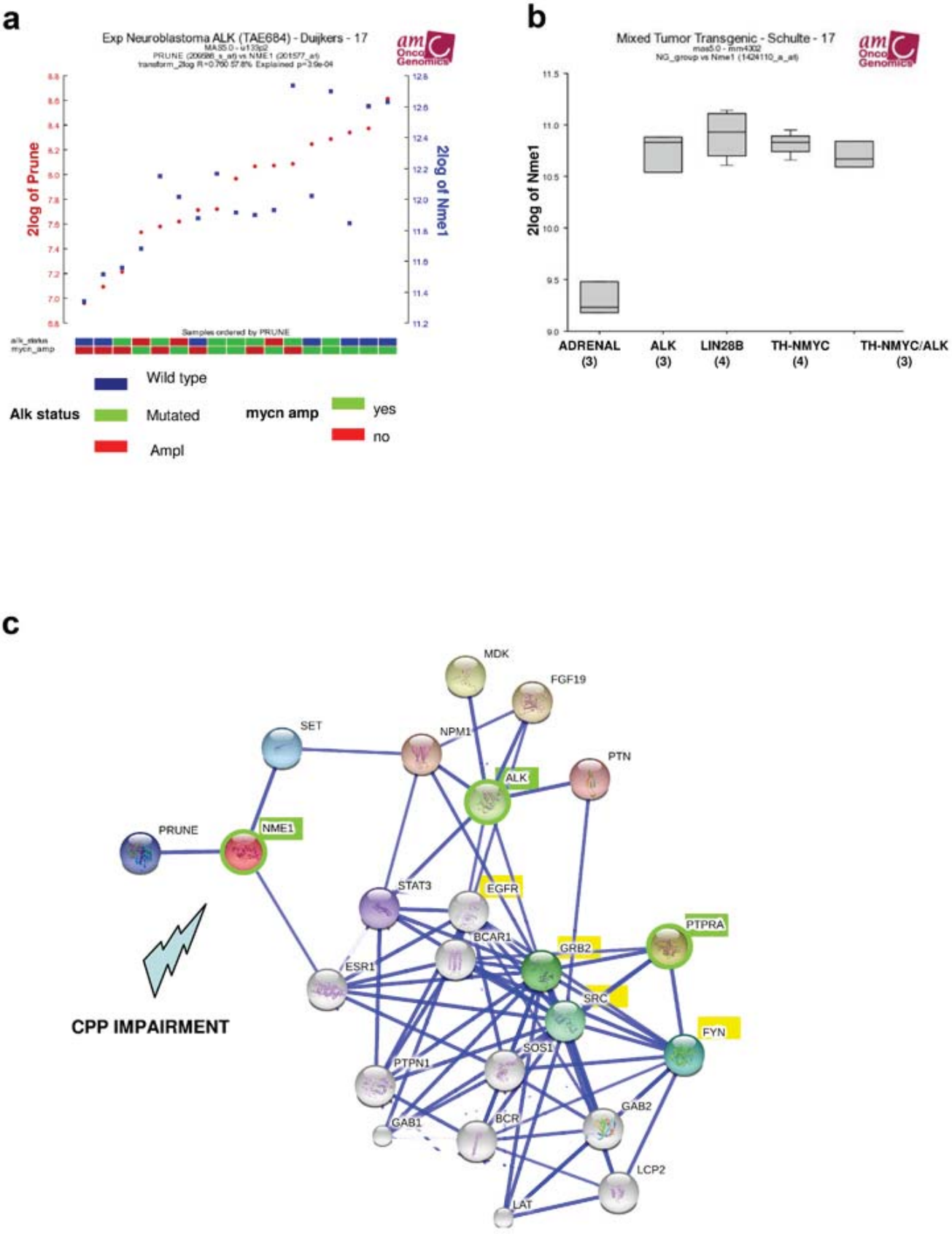
a
Exp Neuroblastoma ALK (TAE684) - Duijkers - 17
2log of Prune
2log of Nme1
Samples ordered by PRUNE
Wild type
Alk status
Mutated
Ampl
mycn amp
yes
no
b
Mixed Tumor Transgenic - Schulte - 17
2log of Nme1
ADRENAL (3)
ALK (3)
LIN28B (4)
TH-NMYC (4)
TH-NMYC/ALK (3)
c
MDK
FGF19
SET
NPM1
PTN
ALK
PRUNE
NME1
STAT3
EGFR
PTPRA
BCAR1
GRB2
ESR1
SRC
FYN
CPP IMPAIRMENT
SOS1
PTPN1
GAB2
GAB1
BCR
LCP2
LAT

Figure S9